RESEARCH ARTICLE

ADVANCED FUNCTIONAL MATERIALS
www.afm-journal.de

All-Material Crosslinked Solid Polymer Electrolytes for High-Performance and Flexible Lithium Metal Battery

*Sung Yeon Bae, Seoyeon Kim, Young Ho Yoo, Jin-Seo Kim, Jieun Lee, Jinhan Cho, Bongjun Yeom, and Jeong Gon Son**

Solid polymer electrolytes (SPE) offer advantages including compatibility with conventional electrolyte systems and mechanical flexibility; however, low ionic conductivity and high interfacial resistance present significant challenges. Here, systems are proposed that randomly crosslink all-materials constituting SPE based on diazide and develop novel flexible SPEs by covalently networking fluorinated polymers and succinonitrile. This all-material crosslinking reduces crystallinity of the constituents, thus simultaneously boosting ionic conductivity, mechanical elasticity, and adhesion strength. Solvent-assisted conformal coating ensures complete contact with the lithium surface and completely wets the porous cathode. The SPE exhibits high ionic conductivities of 4.7 mS·cm^{-1}, lithium-ion transference numbers of 0.64, and oxidation stability up to 5.29 V. It demonstrates stable lithium plating/stripping with ~5 mV of overpotential over 1400 h in Li//Li tests and outstanding performance in Li//LFP flexible full cells, achieving discharge capacities of 136.5 mAh g^{-1} at 3 C and maintained even after bending at 5 mm or cutting in half.

1. Introduction

With the rapidly increasing demand for high energy density Li-ion batteries for applications such as electric vehicles and wearable devices,[1] Li metal anodes with much higher capacity and lower reduction potentials could be a promising solution.[2–5] However, lithium metal batteries (LMBs) have not yet been applied to mass production due to problems such as mechanical instability due to dendrite formation and excessive chemical reactivity with metallic lithium. Especially, the formation of dendrites due to non-uniform ion transfer results in a decrease in Coulombic efficiency due to side reactions occurring in the continuously created solid electrolyte interphase (SEI), and the formation of dead lithium, and the continuous growing dendrites can break through the separator and cause a short circuit, which poses a risk of fire.[6–9]

To address the challenges of LMBs, several strategies[10–16] have been explored, in particular, the use of solid electrolytes that are harder and non-flowable compared to liquid electrolytes to suppress volume expansion and dendrite formation of lithium metal and also enhance battery safety by eliminating flammable organic solvents.[17–19] Among various solid electrolytes, solid polymer electrolytes (SPEs) have recently received a lot of attention from many battery researchers due to their advantages as a polymer material, such as ease of processing, low-pressure fabrication, similarity to general electrolyte systems,[20–22] and further mechanical flexibility[23–25] and deformability. However, compared to liquid or inorganic solid electrolytes, SPEs suffer from low ionic conductivity. Even though polymers can interface better than rigid inorganic electrolytes (due to some compliance under pressure), interfacial contact resistance remains high because of the solid's lack of inherent fluidity. This poor interface lowers Coulombic efficiency and impairs long-term cycling stability, preventing optimal performance.[26,27]

Therefore, several strategies have been proposed in SPE research to increase ionic conductivity and mechanical strength, such as new polymer materials beyond the low-conductivity polyethylene oxide (PEO), incorporation of ceramic fillers, blending of different types of polymers, polymer backbone crosslinking.[28–32] In addition, an in situ polymerization approach has been recently proposed to improve the insufficient

---

S. Y. Bae, S. Kim, Y. H. Yoo, J.-S. Kim, J. Cho, J. G. Son
Electronic and Hybrid Materials Research Center
Korea Institute of Science and Technology
Seoul 02792, Republic of Korea
E-mail: jgson@kist.re.kr

S. Y. Bae, S. Kim, Y. H. Yoo, J. Cho, J. G. Son
KU-KIST Graduate School of Converging Science and Technology
Korea University
Seoul02841, Republic of Korea

J. Lee
Energy Storage Research Center
Korea Institute of Science and Technology
Seoul02792, Republic of Korea

J. Cho
Department of Chemical and Biological Engineering
Korea University
Seoul02841, Republic of Korea

J.-S. Kim, B. Yeom
Department of Chemical Engineering
Hanyang University
Seoul 04763, Republic of Korea

The ORCID identification number(s) for the author(s) of this article can be found under https://doi.org/10.1002/adfm.202508573

DOI: 10.1002/adfm.202508573

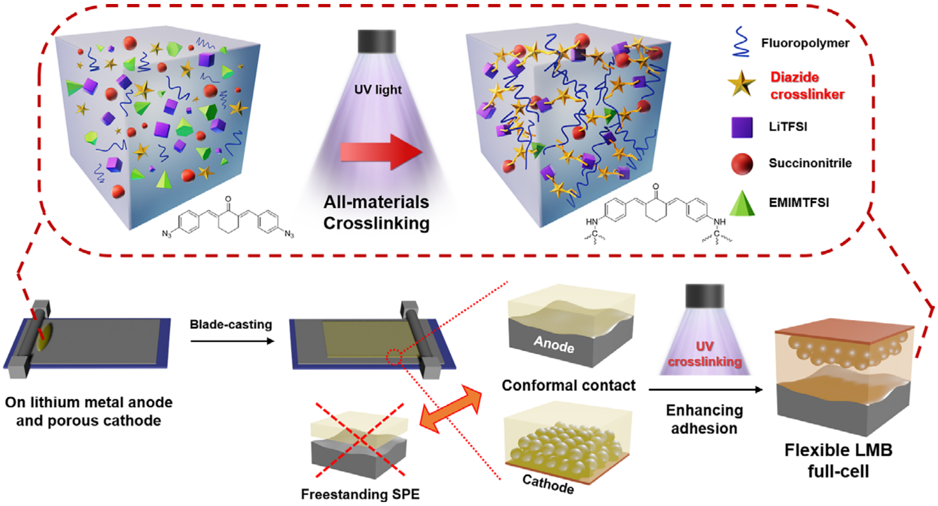

Scheme 1. Schematic diagram of our all-materials crosslinking and fluoropolymer-based SPE and our SPE-based lithium metal battery cell fabrication. The precursor of our SPE was conformally coated on the lithium metal and porous cathode and irradiated with 365 nm UV for 2 min. The flexible full cell was manufactured by stacking the two coated sides of electrodes facing each other and uniting them with light pressure.

interfacial contact between electrodes and electrolytes.[33–38] However, to remain competitive with other solid electrolyte technologies, SPEs still require strategies that simultaneously enhance ionic conductivity and interfacial contact.

Here, we present a uniquely all-component crosslinked SPE that simultaneously boosts ionic conductivity and interfacial contact—a capability not achieved by previous SPE designs. By using a diazide crosslinker that randomly reacts with C—H bonds[39,40] in all components, the diazide crosslinks not only the polymer but also the ion-conductive materials to form a single unified network, which lowers crystallinity and thus simultaneously improves ionic conductivity and mechanical stability. In addition, instead of the commonly used polyethylene oxide, a fluorine-based elastic polymer matrix, which was difficult to crosslink but could be crosslinked using diazide, was used as the framework of the SPE, thereby realizing high electrochemical stability and high ionic conductivity even at room temperature. In addition, unlike conventional methods that require high pressure to attach the electrolyte, we applied our SPE via direct coating onto the lithium foil and the porous cathode, followed by drying and UV cross-linking. After the UV-crosslinks with diazide, this conformally coated SPE tightly adheres the electrolyte to the uneven surface of the lithium metal anode, ensuring uniform lithium-ion flow and suppressing dendrite formation. Unlike typical in situ polymerization that involves polymerizable monomers (e.g., acrylates), our use of a non-polymer specific crosslinker (diazide) means we can solidify a pre-formed electrolyte solution containing stable polymer and additives. This avoids the need for designing special monomers and results in an SPE that is immediately ready after a brief UV exposure. Our SPE effectively stabilizes the lithium metal surface through uniform plating and stripping over 1400 h with an overpotential of 5 mV at 0.1 mA cm^{-2} in Li//Li symmetric cells, a capacity of 130 mAh g^{-1} at 3 C and maintains 98.46% of its capacity after 100 cycles at 1 C in Li//LFP full cells, indicating a promising candidate of high-performance solid-state lithium metal batteries. Even in a lithium metal flexible pouch cell, our deformable SPE operated reliably under very fast charge/discharge conditions of 10 C and maintained its capacity even when bent with a radius of curvature of 5 mm or cut in half, showing excellent performance as an electrolyte material for flexible solid batteries.[41–43]

2. Results and Discussion

Scheme 1 illustrates our all-crosslinking SPE-based direct-coating process for fabricating all-solid-state battery cells. The main components of the solid electrolyte are a fluoropolymer (Poly(vinylidene fluoride-co-hexafluoropropylene), PVDF-HFP) with excellent ion transport in the swelled state, lithium bis(trifluoromethanesulfonyl)imide (LiTFSI) as a lithium-ion source, 1-ethyl-3-methylimidazolium (EMIM)TFSI as an ionic liquid that swells the fluoropolymer well, and succinonitrile, a plastic crystal with excellent lithium-ion transport. These materials are dispersed using dimethyl carbonate (DMC) (Figure S1, Supporting Information), which does not cause side reactions with lithium metal, and a small amount of fluoroethylene carbonate (FEC) for long-term stability, and the electrolyte solution is directly bar-coated onto the lithium metal anode and porous cathode, just as the cathode slurry is coated onto the current collector.

Next, to bind these materials into a single material, a small amount (~1 wt% of solid contents) of a diazide cross-linking reagent, which has been shown to realize high-resolution patterning through ligand cross-linking of long alkyl chains of colloidal quantum dots and light-emitting diodes,[39,40] was introduced. Since diazide crosslinker causes C—H insertion of nitrene upon UV irradiation (Figure S2, Supporting Information) and can react with any materials containing C—H bonds, not just polymer chains, as in random shooting, thereby enabling the creation of solid electrolytes in which all materials are entangled. If all cross-linkers react, ≈1 in 200 can undergo insertion reaction compared to the number of C–Hs in PVDF-HFP and SN, which is a level where PVDF-HFP forms 3~4 bonds per polymer chain. We executed UV irradiation (~0.7 W cm^{-2}) with a

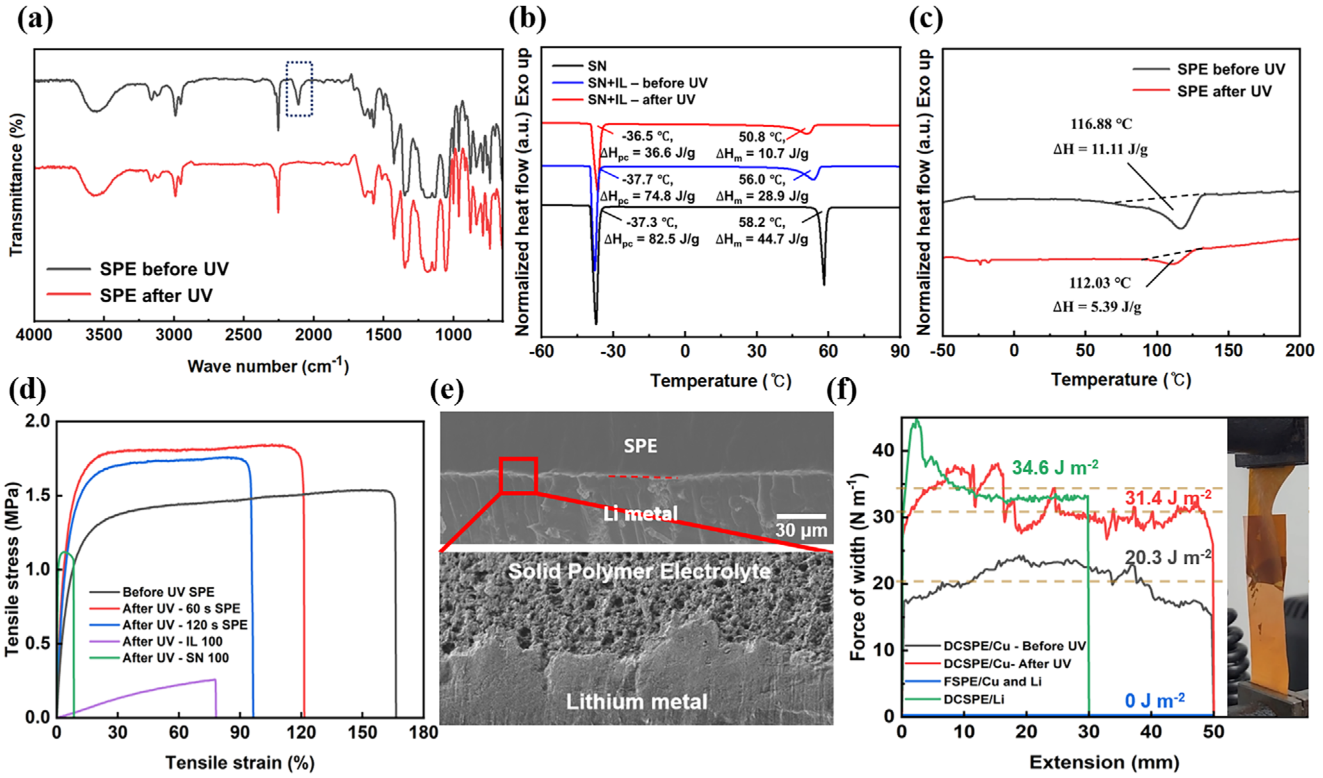

Figure 1. a) FT-IR spectra of the SPE films before (black) and after (red) UV exposure (365 nm, 0.7 W cm^{-2}) for 5 min. b) DSC of succinonitrile (SN) + crosslinker, with (red) and without (black) ionic liquid. c) DSC of the composite SPE (PVDF-HFP + SN + IL + LiTFSI + crosslinker) before (black) and after (red) UV crosslinking for 60 s. d) Stress-strain curves of our SPEs as a function of UV irradiation time and IL-only and SN-only SPEs after UV for 120 s. e) Cross-sectional SEM image of directly coated SPE on Li metal anode after UV for 120 s. f) 180° peel tests for measuring interfacial adhesion between the SPEs and the Cu and Li foil after UV for 120 s. The dotted lines indicate the average force per width.

wavelength of 365 nm from 30 s to 2 min. After UV curing, the cell can be simply assembled by stacking two all-material crosslinked SPE-coated electrodes facing each other and bonding them with light pressure. The thickness of the SPE is controlled to be ≈50 µm.

To examine chemical changes resulting from diazide crosslinking to our solid electrolyte, FT-IR analyses before and after UV irradiation were conducted (**Figure** 1a; Figure S3, Supporting Information). Clearly, the peak associated with N_3- at 2110 cm^{-1} completely disappears after UV exposure, indicating the occurrence of the chemical reaction described in Figure S2 (Supporting Information). This suggests that UV irradiated N_3 in the diazide crosslinker were converted to reactive nitrene intermediates, this intermediate can be inserted into the C—H bonds of the polymer chain and the additive to form interconnections among all components via secondary amine linkages. To evaluate the effect of UV curing on the structural stability of the SPE, a solvent resistance test was conducted using DMC. The uncured sample completely lost its mechanical integrity after immersion in DMC overnight, and the solvent became visibly discolored (Figure S4, Supporting Information), indicating the dissolution of unreacted components. In contrast, the UV-cured sample maintained its shape and remained insoluble in DMC, with no observable change in solvent appearance. These results indicate that UV curing effectively induces chemical crosslinking, resulting in a stable, solvent-resistant network structure.

We performed differential scanning calorimetry (DSC) analysis to confirm the change in crystallinity of SPEs before and after UV irradiation. In Figure 1b, succinonitrile shows a melting point (T_m) of 58.2 °C and a plastic crystal phase transition temperature (T_{pc}) of −37.3 °C. When mixed with an ionic liquid, the T_m slightly decreases to 56.0 °C and the melting enthalpy (ΔH_m) decreases considerably from 44.7 to 28.9 J g^{-1}, but the phase transition peak (T_{pc} and ΔH_{pc}) barely changed. This reveals that physical mixing with ionic liquid hinders the formation of plastic crystals of succinonitrile but does not have a significant effect on real crystal formation. After UV cross-linking, melting related ΔH_m and T_m further decreased to 10.7 J g^{-1} and 50.8 °C, respectively, and phase transition enthalpy (ΔH_{pc}), which previously had no significant change, decreased noticeably by less than half decreased by more than half from 74.8 to 36.6 J g^{-1}. This change is thought to be due to succinonitrile actually being chemically crosslinked by UV and diazide, thereby reducing both plastic crystallinity and real crystallinity at the plastic crystal-to-crystal phase transition. The PVDF-HFP with ionic liquid and diazide crosslinker in Figure S5 (Supporting Information) shows a decreasing melting temperature and crystallinity after the UV crosslinking. The DSC result of our SPE containing PVDF-HFP, succinonitrile, ionic liquid, LiTFSI, and UV cross-linker, shown in Figure 1c, shows that due to the complexation of the SPE before crosslinking, the melting point of PVDF crystals dropped to 117 °C and the crystalline peaks of succinonitrile disappeared.

After the UV, the melting point of PVDF crystals further dropped to 112 °C and the melting enthalpy significantly decreased from 11.1 to 5.4 J g^{-1}, indicating crystallinity of PVDF noticeably decreased after UV cross-linking. These reduced overall crystallinity after UV indicate that random crosslinks formed by C-H insertion of diazide are formed to both PVDF-HFP and succinonitrile. This decrease in crystallinity typically results in more amorphous phases and faster ion movement.

To investigate the change in mechanical properties of the SPEs with UV irradiation, stress-strain curves were obtained using a universal testing machine (UTM), as shown in Figure 1d and Figure S6 (Supporting Information). While the SPE before UV irradiation has Young‘s modulus of 7.7 MPa and could stretch up to 160%, the SPE after 60 s of irradiation exhibited an increased Young‘s modulus of 10.2 MPa, increased by more than 1.3 times. This improvement in mechanical properties is due to the diazide cross-linking agent forming a 3D network structure between solid polymer electrolyte materials through UV irradiation. Comparatively, the SPE containing only PVDF-HFP and only succinonitrile had either too low elastic moduli or were too brittle to be suitable for flexible lithium metal batteries. For evaluating the elasticity of the SPE, the stress-strain curves were measured by repeatedly applying loading and unloading to the SPE while gradually increasing the uniaxial strain, as shown in Figure S7 (Supporting Information). In each strained state, from 10% to 40%, all recovery rates were more than 75%. These high mechanical properties and elasticity allow the SPE to effectively accommodate the volume and morphology changes of lithium metal during cycling.

To analyze the interfacial properties of our SPE with lithium metal and the porous cathode, cross-sections of the SPE coated on both the lithium metal and the cathode, which were cut by ion beam, were examined by SEM. Only an intimate interface without gaps was observed between the lithium metal anode and the electrolyte after cutting (Figure 1e), and it also shows that the solid electrolyte penetrates into the porous structure to ensure uniform contact with the LFP cathode (Figure S8, Supporting Information). Direct casting on the electrodes in a liquid state ensures sufficient wetting, and even after the solvent evaporates and transitions to a solid state, the film remains conformally attached (intimately in contact) to the rough electrode surface without delamination. After the electrolyte coating, no unevenness or bubbles were observed on the surfaces of each electrode (Figure S9, Supporting Information) and if the two electrodes are attached and then pressure is applied with a weight and annealed on a hot plate at ≈60 °C for 30 min, the interface between the same materials disappears enough to cause cohesive fracture upon separation.

For evaluating interfacial adhesion property, a 180° peel-off strength test was conducted (Figure 1f). The freestanding film SPE did not adhere to the Cu foil and easily separated (Figure S10, Supporting Information), whereas directly coated SPE exhibited a high adhesion energy of 20.3 J m^{-2} before UV crosslinking. Moreover, after UV crosslinking, the average adhesion energy further increased to 31.4 J m^{-2} and some residue remained on the Cu foil after peeling (inset image of Figure 1f), indicating a strong interfacial bond that leads to cohesive failure within the electrolyte. In the peeling experiment with Li foil, an even higher interfacial adhesion of 34.6 J m^{-2} and partial residue on the lithium metal was also observed (Figure S11, Supporting Information). In addition, even after 5 cycles in a Li//Li symmetric cell, the adhesion properties with Li metal were excellently maintained at a very high value of 24.5 J m^{-2} (Figure S12, Supporting Information). Considering that the required adhesion energy to form a stable interface capable of withstanding mechanical stress during cell operation is ∼5 J m^{-2}, this demonstrates sufficient interfacial stability. This improved adhesion is because UV cross-linking induces a chemical reaction at the electrode interface, which can allow the interface to remain stable even during repeated charging/discharging and bending of the flexible battery.

With the SPE's mechanical robustness and adhesion confirmed, we next examined its ionic transport properties. **Figure 2a** shows the ionic conductivity of the SPE as a function of UV curing time. The SPE before UV curing showed a high ionic conductivity of ∼2.7 mS•cm^{-1} at room temperature, which is due to the high ionic conductivity of fluoropolymer swollen in ionic liquid at room temperature[44–47] and another highly conductive succinonitrile. Additionally, as the curing time increased to 120 s, the ionic conductivity further increased to 5.4 mS·cm^{-1}, indicating that the cross-linking through the C—H bond insertion reaction of diazide effectively suppresses the crystallization of polymers and succinonitrile and facilitates ion transport. Extending UV exposure beyond 120 s caused the ionic conductivity to decrease, likely because excessive cross-linking immobilizes the polymer matrix. The irradiation time for all subsequent experiments was fixed at 120 s. By controlling the ratio of the ionic liquid and succinonitrile, the roles of the two could be confirmed. As the ionic liquid ratio increased, the ionic conductivity increased (Figure S13, Supporting Information), and when the lithium-ion transfer number t_{Li+} was measured by the Bruce–Vincent method, t_{Li+} increased with increasing the succinonitrile content (Figure S14, Supporting Information). Considering both the ionic conductivity and the t_{Li+} of the SPE, we optimized the ratio of the ionic liquid and succinonitrile to 1:2 ratio (Figure S15, Supporting Information)[48] and overall mass ratio of PVDF-HFP:IL:SN:LiTFSI was optimized to 1:1.5:3:0.6 considering not only the ionic conductivity and lithium ion transfer number but also the mechanical properties. The t_{Li+} at the 1:2 ratio was 0.64 (Figure 2b), which is relatively higher than that of conventional organic liquid electrolytes (0.2∼0.4) or most solid polymer electrolytes (often 0.4–0.5) , showing that rapid charging and discharging is possible in LMB without concentration depletion.[49–51] We summarize and compare the performance of several developed solid polymer electrolytes with our SPE in Table S2 (Supporting Information).

Linear sweep voltammetry (LSV) and cyclic voltammetry (CV) tests were performed to evaluate the electrochemical stability and reversibility of the SPE, as shown in Figure 2c and Figure S16 (Supporting Information), respectively. No significant oxidative current was observed until 5.3 V, indicating all SPE components (fluoropolymer, succinonitrile, ionic liquid) remain inert in the operating range of common cathodes. The oxidation onset voltage before UV cross-linking was 4.92 V, but after curing it increased to 5.29 V due to the consumption of reactive moieties during cross-linking. The CV results exhibited overlapping profiles from the 2nd to the 10th cycle, indicating highly reversible electrochemical behavior of the electrolyte. Additionally, electrochemical impedance spectroscopy (EIS) analysis was performed

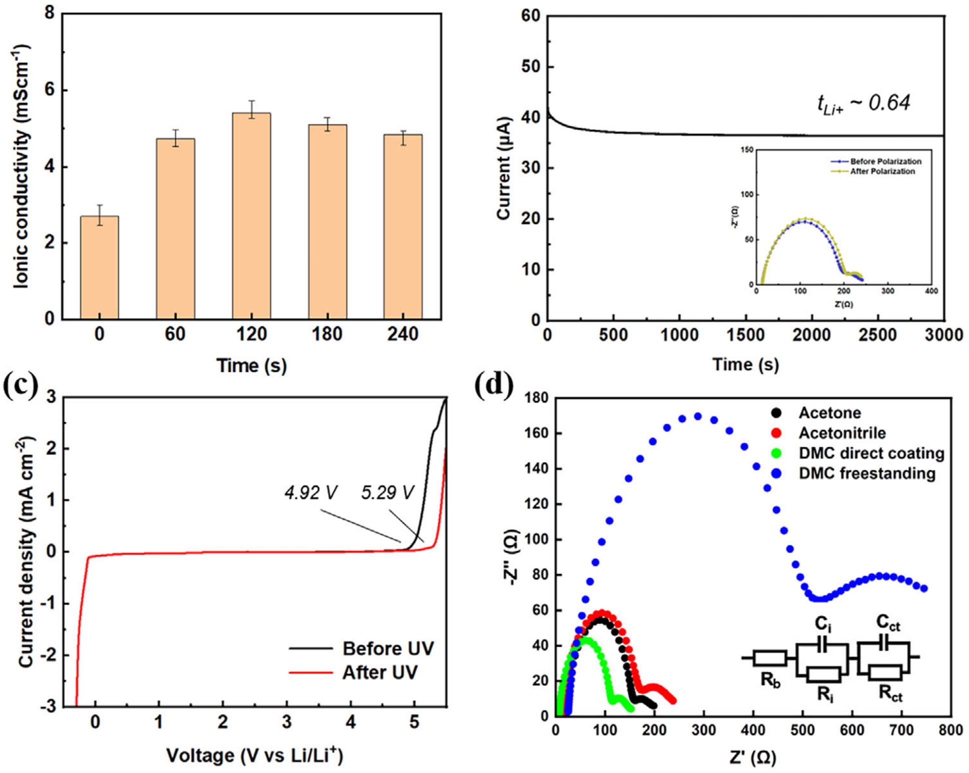

Figure 2. a) Measured ionic conductivities of the SPEs with various UV irradiation time. b) Lithium-ion transference number t_{Li+} of 1:2 ratio of ionic liquid and succinonitrile measured using the Bruce-Vincent method. c) Linear sweep voltammetry (LSV) profile of the SPE before and after UV irradiation for measuring electrochemical stability window. d) Nyquist plots of symmetric Li cells with free-standing film electrolyte and directly coated electrolyte with DMC, acetone and acetonitrile.

on lithium symmetric cells using our SPE in different forms: i) directly coated on Li (with different casting solvents) and ii) as a free-standing film (same composition and thickness) (Figure 2d). For the freestanding SPE film, the bulk resistance (R_b) and interfacial resistance (R_i) showed large values of 25 Ω and 540 Ω, respectively, whereas for the direct coating electrolyte, acetone (18 Ω, 157 Ω) and acetonitrile (11 Ω, 176 Ω), which showed slight side reactions, showed slightly lower values, and in particular, DMC, which showed almost no side reactions, showed very low values of 7 Ω and 113 Ω for R_b and R_i, respectively. Since DMC does not react with Li metal, it preserved a low interfacial resistance. In addition, unlike liquid electrolytes, the crosslinked SPE does not ignite (Movie S1, Supporting Information) because most of the DMC solvent evaporates during the drying process, highlighting its safety.

Using our SPE as the solid electrolyte in an actual battery, lithium plating and stripping tests performed on lithium symmetric cells (**Figure** 3a; Figures S17 and S18, Supporting Information). The liquid electrolyte and freestanding SPE exhibited an initial voltage arch followed by a plateau with relatively high overpotentials, and short-circuited after 640 and 1150 h, respectively. Even with direct coating, when only succinonitrile was contained in the SPE, the overpotential increased and formed an arched profile, which is thought to be due to a side reaction between succinonitrile and lithium metal. The SPE containing only ionic liquids exhibited a much higher overpotential and short cycle life due to its low mechanical strength without a separator in the cell. However, our mixed SPE cell maintained a flat profile, and exhibited excellent cycling performance with a low polarization of 5 mV for over 1400 h at a current density of 0.1 mA cm^{-2}, after which the overpotential increased and a short circuit finally occurred. The directly coated SPE exhibits two times longer cell lifespan and superior overpotential performance compared to commercially used liquid electrolytes. This excellent stability can be attributed to the SPE's high ionic conductivity (which minimizes concentration polarization), its elasticity and strong adhesion (which accommodate lithium volume changes and prevent interface delamination), as well as the uniform lithium-ion flux enabled by the conformal electrolyte interface. In addition, when charge and discharge were performed at 0.05 mA cm^{-2} increments to measure the critical current density in Figure 3b, a short-circuit occurred only when the current reached 0.65 mA cm^{-2}. To investigate the compatibility between lithium metal and electrolyte, the interfacial resistance of the lithium symmetric cell was measured after 70 days and maintained a value of 130 Ω (Figure S19, Supporting Information).

We also compared the morphologies of lithium metal surfaces (Figure 3c–e; Figures S20–S23, Supporting Information) using various electrolytes after 100 cycles. The liquid electrolyte with a conventional separator resulted in rough and porous lithium metal surface, including dendrites, dead lithium, and mossy structures (Figure 3c) and the surface with free-standing SPE was relatively smooth but some irregularities and moss structures

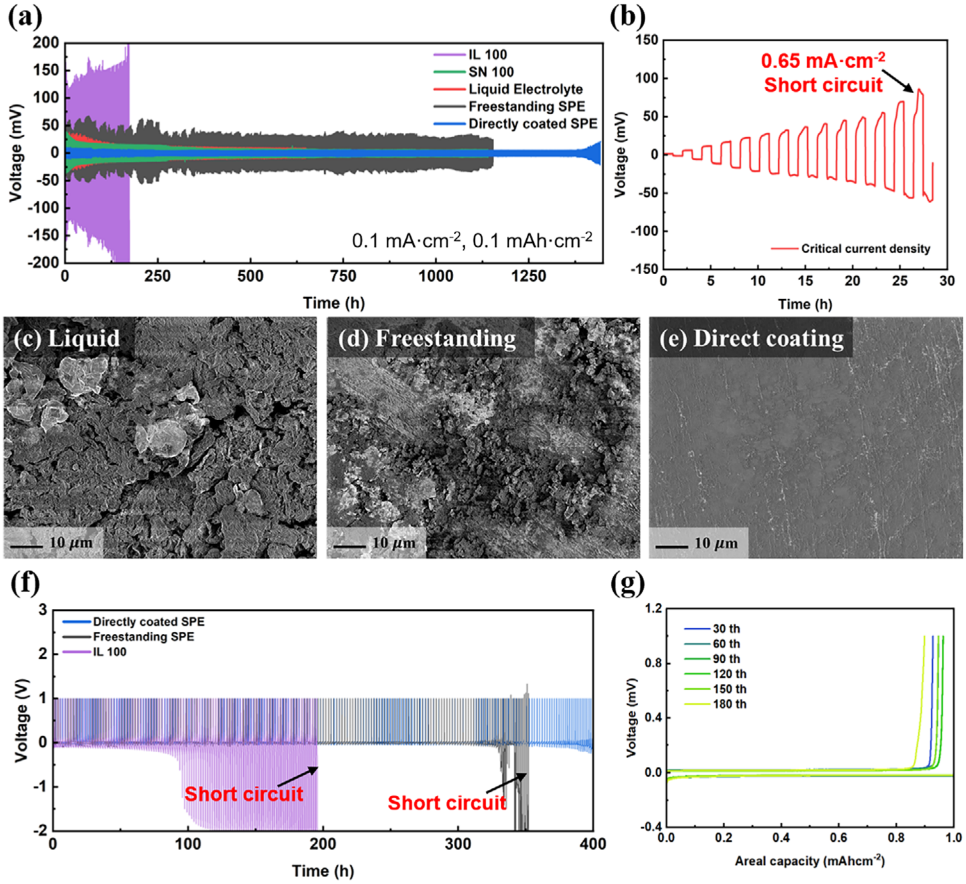

Figure 3. a) The cycling performance of the Li symmetric cells with liquid electrolyte, SPE with free-standing and direct coating configurations (including IL-only and SN-only SPEs) at 0.1 mA cm^{-2} and 0.1 mAh cm^{-2} and b) critical current density with 0.05 mA cm^{-2} increments. c–e) SEM images of the Li metal anode after 100 cycles at 0.1 mA cm^{-2} with c) liquid electrolyte, d) freestanding SPE and e) directly coated SPE. f) The cycling performance of the asymmetric Li//Cu cell with directly coated SPE (mixed and IL-only) and freestanding SPE at current density of 0.1 mA cm^{-2} with capacity of 0.1 mAh cm^{-2}. g) Corresponding voltage profiles for different cycling.

were formed (Figure 3d). In contrast, the lithium surface with directly coated SPE showed a much smoother surface without previously observed stripes (Figure 3e). In addition, X-ray photoelectron spectroscopy (XPS), analysis of this surface (Figure S24, Supporting Information) showed that a significant portion of the formed SEI at lithium surface was composed of Li-F, indicating excellent interfacial stability by forming a LiF-rich SEI from abundant fluorine sources of fluoropolymers, FEC and TFSI anions. In addition, the XPS full scan spectra (Figure S25, Supporting Information) and element fractions of lithium surface (Table S1, Supporting Information) with free-standing and directly coated SPE showed that the directly coated sample had a relatively lower fraction of O and higher fraction of F compared to the free-standing sample. These surface analyses show that the SPE can stabilize lithium metal surfaces more efficiently than liquid electrolytes during the charge-discharge process and can induce a more uniform lithium-ion flux.

The variously prepared SPE also demonstrated high stability and cycling performance, even in an asymmetric Li//Cu cell (Figure 3f; Figure S26, Supporting Information). At a current density of 0.1 mA cm^{-2} and an areal capacity of 0.1 mAh cm^{-2}, the Li//Cu cell with our SPE stably operated for over 200 cycles with a low overpotential of less than 25 mV. Enlarged views of the voltage profiles (Figure S27, Supporting Information) show maintaining a flat plateau with an overpotential of 25 mV during both the plating and stripping processes at early, middle, and late times over 350 h. Voltage profiles at various cycles (Figure 3g) also indicate the SPE exhibits reversible plating-stripping behavior even after 180 cycles.

Then, we investigated the performance in full cells through the application of LFP cathodes in LMB. Since porous cathode requires complete contact with the electrolyte, the ultra-high-pressure process or mixing a certain amount of solid electrolyte into the cathode paste (e.g. 7:1:1:1 of weight ratio) is attempted, but the content of the active material is inevitably reduced accordingly. Our coating method forms conformal interfaces, so it has the advantage of not only lowering the interfacial resistance but also maximizing the content of the active material at a 9:0.5:0.5 level. We fabricated our SPE-based solid state LFP//Li metal full cell by pressing the SPE-coated side of the cathode against the SPE-coated lithium metal anode. **Figure 4a,b** demonstrates that in a full cell LMB using an LFP cathode, a discharge capacity of 165 mAh g^{-1} was maintained at 1 C for 100 cycles at 20 °C (98.46% of capacity retention) and a low overpotential of 70 mV

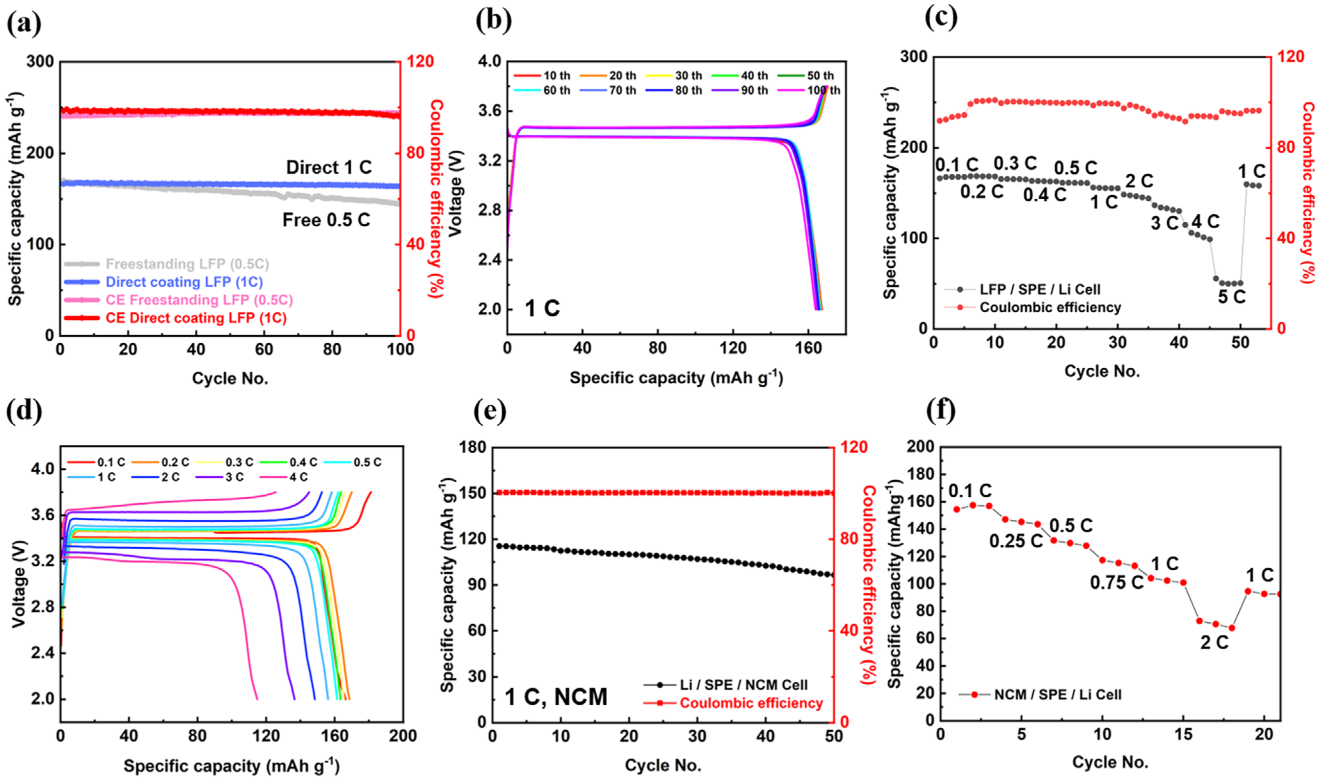

Figure 4. a) The cycling performance of our SPE based LFP//Li metal full cell as a function of cycle number in the voltage range of 2.0–3.8 V. b) Corresponding voltage profiles at each cycle. c) Rate capability of the LFP full cell in the voltage range of 2.0–3.8 V from 0.1 C to 5 C, 5 cycles for each C-rates. d) Corresponding voltage profiles at each C-rate. e) The cycling performance at 1 C and f) rate capability of NCM/SPE/Li metal full cell.

without significant capacity loss. Moreover, the rate capability of the cell was evaluated at different C-rates ranging from 0.1 C to 5 C (Figure 4c,d). At a high C-rate of 3 and 4 C, the cell achieved capacities of 130 and 99 mAh g^{-1}, respectively, which are 79% and 60% of its capacity at 0.1 C, indicating some transport limitations but still excellent relative to other SPE systems. In addition, the high capacity was maintained even at high loading of ~5 mg cm^{-2} (Figure S28, Supporting Information). This result is a very high rate capability among reported polymer-based solid electrolytes,[23–25] which often suffer at high C-rates due to lower ionic conductivities, especially considering it is achieved at room temperature. The full-cell with NCM811-based cathode (Figure 4e,f) also exhibited a capacity of more than 100 mAh g^{-1} after 50 cycles at 1 C and decent rate capability, demonstrating fast charge/discharge performance even at high voltages. However, the IL-only and SN-only SPEs show no ability to cycle at 1 C after an initial charge-discharge at 0.1 C (Figure S29, Supporting Information).

Finally, to evaluate the commercial viability of our SPE beyond coin cells, we fabricated the lithium metal battery with pouch cell configuration (inset images in **Figure 5a**; Figure S30, Supporting Information) and assessed electrochemical performance, mechanical durability and safety. As shown in Figure 5a, a Li/SPE/LFP pouch cell exhibited stable cycling performance at 0.5 C, maintaining a capacity of 130 mAh g^{-1} over 100 cycles. High-rate charge/discharge performance was also evaluated; Figure 5b demonstrates stable voltage profiles over 150 cycles at 2 C-rate. Rate capacity tests (Figure 5c) show good performance from 1 C up to very high rate of 10 C, indicating significant ionic conductivity even in the SPE-based pouch cell, enabling efficient lithium-ion transport at high rates. The all-material crosslinking and direct coating contributes to stable interface formation, minimizing resistance and enabling high-rate cycling performance, confirming the SPE's suitability for both coin and pouch cells. Similarly, the Li/SPE/NCM cell showed a capacity retention of 92.1% after 30 cycles at 0.5 C with a high average coulombic efficiency of 99.2% (Figure 5d), highlighting the ability to provide a stable and reliable platform for reversible lithium-ion insertion in both LFP and NCM configurations.

To investigate the performance of our SPE-based pouch cells under various physical deformation, we conducted cut and bend tests. Figure 5e shows that even after cutting the Li/SPE/LFP cell in half, stable cycling performance was sustained over 30 cycles in the remaining area, indicating high electrochemical stability even under physical damage. Additionally, the cell demonstrated the ability to power an LED after being folded and cut multiple times (Figure S31, Supporting Information). This robustness, achieved without any separator, offers significant safety advantages over traditional liquid electrolyte-based lithium-metal batteries by mitigating fire hazards. Furthermore, Figure 5f,g show that the pouch cell clamped on the jig showed minimal changes in both specific capacity and voltage under both flat and bent conditions up to a curvature of 5 mm, suggesting that the all-material cross-linking and direct coating provide strong adhesion between

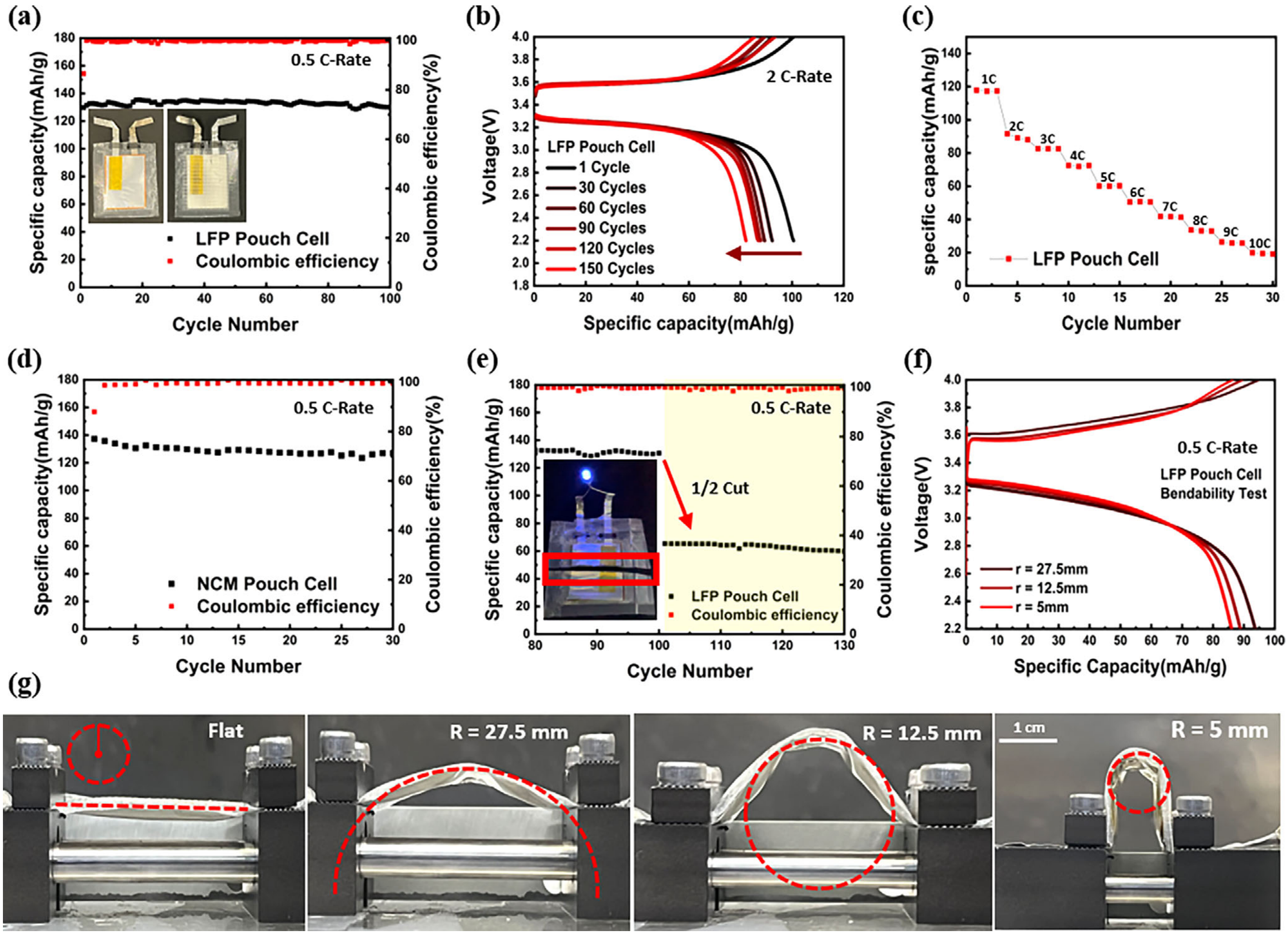

Figure 5. a) Li metal/SPE/LFP Pouch cell over 100 cycles at a 0.5 C-rate. b) Voltage profiles of the LFP pouch cell during cycling at 2 C-rate across multiple cycles. c) Rate capability test for the LFP pouch cell at increasing C-rates from 1 C to 10 C. d) NCM pouch cell over 30 cycles at 0.5 C-rate. e) LFP pouch cell before and after undergoing a 1/2 cut test at 0.5 C. The inset image shows a well-operated (lighting a LED) pouch cell even after being cut. f) For the flexibility test, voltage profiles for the LFP pouch cell under different bending curvatures. g) Photographic images of the LFP pouch cell bent to different radius of curvature, demonstrating the flexibility and structural resilience of the cell.

the layers. This strong interlayer adhesion allows the entire cell to deform as a single object, maintaining mechanical integrity and electrochemical performance even under bending. Notably, these extreme tests (cutting, repeated folding) would be catastrophic for conventional liquid-based cells, whereas our solid-state cell survives due to the solid electrolyte's cohesion and non-flammable nature. The performance comparison between our study and other flexible Li metal batteries[23–25] is summarized in the Table S3 (Supporting Information). To our knowledge, this is one of the first solid-state Li metal batteries to demonstrate full functionality even after being cut in half, and one of very few to retain ~100% capacity after bending to a small radius . Prior studies of flexible Li metal batteries mostly used liquid electrolytes and did not test such extreme mechanical deformations.

3. Conclusion

In summary, this work combines, for the first time, an all-component crosslinking strategy with a direct coating process, yielding a solid polymer electrolyte that simultaneously offers liquid-like ionic conductivity, high lithium transference, strong interfacial adhesion, and mechanical deformability. These combined properties enable unprecedented performance in flexible lithium metal batteries, distinguishing our approach from earlier SPE designs. In particular, in our SPE, PVDF-HFP provides mechanical stability and high-voltage stability, SN provides high ionic conductivity, IL provides ambient ionic conductivity and plasticization, and the diazide crosslinker synergistically ties it all together enhancing all aspects. The SPEs produced through a straightforward and uniform process exhibited excellent cycling performance with low overpotential in both symmetric Li//Li cells and asymmetric Li//Cu cells. Furthermore, in lithium metal battery (LMB) full cell tests, the SPEs demonstrated outstanding performance of high-rate capability and prolonged cycle life at room temperature. When fabricated as pouch cells, it performed well even at high charge/discharge rates of 10 C and maintained their performance even when cut or bent down to 5 mm, demonstrating remarkable performance for flexible Li metal batteries. This all-material crosslinking strategy provides a versatile platform for next-generation solid-state batteries, especially for flexible or wearable applications, by enabling high-performance SPEs across various polymer chemistries and electrode configurations.

Supporting Information

Supporting Information is available from the Wiley Online Library or from the author.

Acknowledgements

S.Y.B., S.K., and Y.H.Y. contributed equally to this work. The authors gratefully acknowledge financial support from the Korea Institute of Science and Technology (KIST) Institutional Program and KU-KIST program, and the National Research Foundation of Korea (NRF) grant funded by the Ministry of Science and ICT of Korea government (No. RS-2024-00451691).

Conflict of Interest

The authors declare no conflict of interest.

Data Availability Statement

The data that support the findings of this study are available from the corresponding author upon reasonable request.

Keywords

all-materials crosslinking, flexible battery, interfacial contact, lithium metal batteries, solid polymer electrolytes

Received: April 4, 2025
Revised: May 12, 2025
Published online:

---

[1] J. W. Choi, D. Aurbach, *Nat. Rev. Mater.* **2016**, *1*, 16013.
[2] L. Sun, Y. Liu, R. Shao, J. Wu, R. Jiang, Z. Jin, *Energy Storage Mater.* **2022**, *46*, 482.
[3] L. Grande, E. Paillard, J. Hassoun, J. Park, Y. Lee, Y. Sun, S. Passerini, B. Scrosati, *Adv. Mater.* **2015**, *27*, 784.
[4] B. Liu, J.-G. Zhang, W. Xu, *Joule* **2018**, *2*, 833.
[5] S. Kim, G. Park, S. J. Lee, S. Seo, K. Ryu, C. H. Kim, J. W. Choi, *Adv. Mater.* **2023**, *35*, 2206625.
[6] Z. Ning, G. Li, D. L. R. Melvin, Y. Chen, J. Bu, D. Spencer-Jolly, J. Liu, B. Hu, X. Gao, J. Perera, C. Gong, S. D. Pu, S. Zhang, B. Liu, G. O. Hartley, A. J. Bodey, R. I. Todd, P. S. Grant, D. E. J. Armstrong, T. J. Marrow, C. W. Monroe, P. G. Bruce, *Nature* **2023**, *618*, 287.
[7] J. Qian, W. A. Henderson, W. Xu, P. Bhattacharya, M. Engelhard, O. Borodin, J.-G. Zhang, *Nat. Commun.* **2015**, *6*, 6362.
[8] J. H. Um, S. Yu, *Adv. Energy Mater.* **2021**, *11*, 2003004.
[9] J. Park, S. Ha, J. Y. Jung, J. Hyun, S. Yu, H. Lim, N. D. Kim, Y. S. Yun, *Adv. Sci.* **2022**, *9*, 2104145.
[10] Y. Wang, Y. Liu, M. Nguyen, J. Cho, N. Katyal, B. S. Vishnugopi, H. Hao, R. Fang, N. Wu, P. Liu, P. P. Mukherjee, J. Nanda, G. Henkelman, J. Watt, D. Mitlin, *Adv. Mater.* **2023**, *35*, 2206762.
[11] S. Kandula, E. Kim, C. W. Ahn, J. Lee, B. Yeom, S. W. Lee, J. Cho, H.-K. Lim, Y. Lee, J. G. Son, *Energy Storage Mater.* **2023**, *63*, 103024.
[12] Y. J. Gong, S. Pyo, H. Kim, J. Cho, H. Yun, H. Kim, S. Ryu, J. Yoo, Y. S. Kim, *Energy Environ. Sci.* **2021**, *14*, 940.
[13] S. Pyo, S. Ryu, Y. J. Gong, J. Cho, H. Yun, H. Kim, J. Lee, B. Min, Y. Choi, J. Yoo, Y. S. Kim, *Adv. Energy Mater.* **2023**, *13*, 2203573.
[14] W. Liu, P. Liu, D. Mitlin, *Adv. Energy Mater.* **2020**, *10*, 2002297.
[15] S. Han, Z. Li, Y. Zhang, D. Lei, C. Wang, *Energy Storage Mater.* **2022**, *48*, 384.
[16] Y. Li, J. Li, H. Xiao, T. Xie, W. Zheng, J. He, H. Zhu, S. Huang, *Adv. Funct. Mater.* **2023**, *33*, 2213905.
[17] S. Xia, X. Wu, Z. Zhang, Y. Cui, W. Liu, *Chem* **2019**, *5*, 753.
[18] Y. Shen, Y. Zhang, S. Han, J. Wang, Z. Peng, L. Chen, *Joule* **2018**, *2*, 1674.
[19] X.-B. Cheng, C.-Z. Zhao, Y.-X. Yao, H. Liu, Q. Zhang, *Chem* **2019**, *5*, 74.
[20] H. Wang, L. Sheng, G. Yasin, L. Wang, H. Xu, X. He, *Energy Storage Mater.* **2020**, *33*, 188.
[21] S. Choudhury, S. Stalin, D. Vu, A. Warren, Y. Deng, P. Biswal, L. A. Archer, *Nat. Commun.* **2019**, *10*, 4398.
[22] G. Xi, M. Xiao, S. Wang, D. Han, Y. Li, Y. Meng, *Adv. Funct. Mater.* **2021**, *31*, 2007598.
[23] D. Guo, D. B. Shinde, W. Shin, E. Abou-Hamad, A. Emwas, Z. Lai, A. Manthiram, *Adv. Mater.* **2022**, *34*, 2201410.
[24] J. Wan, J. Xie, X. Kong, Z. Liu, K. Liu, F. Shi, A. Pei, H. Chen, W. Chen, J. Chen, X. Zhang, L. Zong, J. Wang, L.-Q. Chen, J. Qin, Y. Cui, *Nat. Nanotechnol.* **2019**, *14*, 705.
[25] S. Kim, N. Kim, U. Choe, J. Kim, Y. Lee, S. Lee, *Adv. Energy Mater.* **2021**, *11*, 2100531.
[26] F. Wu, K. Zhang, Y. Liu, H. Gao, Y. Bai, X. Wang, C. Wu, *Energy Storage Mater.* **2020**, *33*, 26.
[27] Z. Song, F. Chen, M. Martinez-Ibañez, W. Feng, M. Forsyth, Z. Zhou, M. Armand, H. Zhang, *Nat. Commun.* **2023**, *14*, 4884.
[28] D. Zhang, L. Zhang, K. Yang, H. Wang, C. Yu, D. Xu, B. Xu, L. M. Wang, *ACS Appl. Mater. Interfaces* **2017**, *9*, 36886.
[29] Y. Zhang, W. Lu, L. Cong, J. Liu, L. Sun, A. Mauger, C. M. Julien, H. Xie, J. Liu, *J. Power Sources* **2019**, *420*, 63.
[30] L. Tang, B. Chen, Z. Zhang, C. Ma, J. Chen, Y. Huang, F. Zhang, Q. Dong, G. Xue, D. Chen, C. Hu, S. Li, Z. Liu, Y. Shen, Q. Chen, L. Chen, *Nat. Commun.* **2023**, *14*, 2301.
[31] S. Liu, W. Liu, D. Ba, Y. Zhao, Y. Ye, Y. Li, J. Liu, *Adv. Mater.* **2023**, *35*, 2110423.
[32] R. Xu, S. Xu, F. Wang, R. Xiao, P. Tang, X. Zhang, S. Bai, Z. Sun, F. Li, *Small Struct.* **2023**, *4*, 2200206.
[33] Y. Cho, C. Hwang, D. S. Cheong, Y. Kim, H. Song, *Adv. Mater.* **2019**, *31*, 1804909.
[34] K. Mu, D. Wang, W. Dong, Q. Liu, Z. Song, W. Xu, P. Yao, Y. Chen, B. Yang, C. Li, L. Tian, C. Zhu, J. Xu, *Adv. Mater.* **2023**, *35*, 2304686.
[35] M. J. Lee, J. Han, K. Lee, Y. J. Lee, B. G. Kim, K.-N. Jung, B. J. Kim, S. W. Lee, *Nature* **2022**, *601*, 217.
[36] J. Han, M. J. Lee, J. H. Min, K. H. Kim, K. Lee, S. H. Kwon, J. Park, K. Ryu, H. Seong, H. Kang, E. Lee, S. W. Lee, B. J. Kim, *Adv. Funct. Mater.* **2024**, *34*, 2310801.
[37] J. Park, H. Seong, C. Yuk, D. Lee, Y. Byun, E. Lee, W. Lee, B. J. Kim, *Adv. Mater.* **2024**, *36*, 2403191.
[38] H. Peng, T. Long, J. Peng, H. Chen, L. Ji, H. Sun, L. Huang, S. Sun, *Adv. Energy Mater.* **2024**, *14*, 2400428.
[39] R. Q. Png, P. J. Chia, J. C. Tang, B. Liu, S. Sivaramakrishnan, M. Zhou, S. H. Khong, H. S. O. Chan, J. H. Burroughes, L. L. Chua, R. H. Friend, P. K. H. Ho, *Nat. Mater.* **2010**, *9*, 152.
[40] J. Yang, D. Hahm, K. Kim, S. Rhee, M. Lee, S. Kim, J. H. Chang, H. W. Park, J. Lim, M. Lee, H. Kim, J. Bang, H. Ahn, J. H. Cho, J. Kwak, B. Kim, C. Lee, W. K. Bae, M. S. Kang, *Nat. Commun.* **2020**, *11*, 2874.
[41] Z. Wang, L. Shen, S. Deng, P. Cui, X. Yao, *Adv. Mater.* **2021**, *33*, 2100353.

[42] F. Xu, S. Deng, Q. Guo, D. Zhou, X. Yao, *Small Methods* **2021**, *5*, 2100262.
[43] Z. Wang, Q. Guo, R. Jiang, S. Deng, J. Ma, P. Cui, X. Yao, *Chem. Eng. J.* **2022**, *435*, 135106.
[44] G. P. Pandey, S. A. Hashmi, *J. Mater. Chem. A Mater.* **2013**, *1*, 3372.
[45] W. Chen, Z. Xing, Y. Wei, X. Zhang, Q. Zhang, *Polymer* **2023**, *268*, 125727.
[46] M. Y. Bhat, N. Yadav, S. A. Hashmi, *Electrochim. Acta* **2019**, *304*, 94.
[47] T. Zhou, Y. Zhao, J. W. Choi, A. Coskun, *Angew. Chem., Int. Ed.* **2021**, *60*, 22791.
[48] A.-H. Ban, S.-J. Pyo, W. J Bae, H.-S. Woo, J. Moon, D.-W. Kim, *Chem. Eng. J.* **2023**, *475*, 146266.
[49] K. Timachova, H. Watanabe, N. P. Balsara, *Macromolecules* **2015**, *48*, 7882.
[50] K. M. Diederichsen, E. J. McShane, B. D. McCloskey, *ACS Energy Lett.* **2017**, *2*, 2563.
[51] P. G. Bruce, J. Evans, C. A. Vincent, *Solid State Ion* **1988**, *28–30*, 918.